nature neuroscience

Bump attractor dynamics in prefrontal cortex explains behavioral precision in spatial working memory

Klaus Wimmer[1], Duane Q Nykamp[1,2], Christos Constantinidis[3] & Albert Compte[1]

Prefrontal persistent activity during the delay of spatial working memory tasks is thought to maintain spatial location in memory. A 'bump attractor' computational model can account for this physiology and its relationship to behavior. However, direct experimental evidence linking parameters of prefrontal firing to the memory report in individual trials is lacking, and, to date, no demonstration exists that bump attractor dynamics underlies spatial working memory. We analyzed monkey data and found model-derived predictive relationships between the variability of prefrontal activity in the delay and the fine details of recalled spatial location, as evident in trial-to-trial imprecise oculomotor responses. Our results support a diffusing bump representation for spatial working memory instantiated in persistent prefrontal activity. These findings reinforce persistent activity as a basis for spatial working memory, provide evidence for a continuous prefrontal representation of memorized space and offer experimental support for bump attractor dynamics mediating cognitive tasks in the cortex.

The neural basis of spatial working memory has been studied extensively with oculomotor delayed response tasks in awake behaving monkeys[1–3]. Experiments have reported persistent neural activity in prefrontal cortex (PFC) during the delay period after a spatial stimulus and before the memory-guided saccadic response. Notably, this neural activity is selective to the location of the visual cues, and the persistent activity can be described as a function of stimulus position using a bell-shaped tuning curve[2]. These observations suggest that a continuous spatial representation in PFC, persisting during the delay period, could underlie spatial working memory. However, assumptions necessary to link this neuronal code with behavior have yet to be validated by experimental data.

Continuous, persistent population codes emerge naturally in computational models of the cortical microcircuit, typically by combining local recurrent excitation and broader feedback inhibition[4–8]. Such network models can display a bell-shaped pattern of activity (bump) even in the absence of tuned external input, known as a bump attractor because the network structure causes neural activity to be naturally attracted toward the bump state. The bump attractor has been proposed to be the network substrate underlying spatial working memory because of two main features. First, the self-sustained attractor in the absence of tuned external input is precisely the condition required for tuned persistent activity during the stimulus-devoid delay period. Second, the center of the bump can be located at any continuously varying location across the network; thus, the bump location provides a substrate for encoding a continuous variable such as spatial location.

In the absence of direct experimental evidence for this model, it has been a matter of debate whether activity in PFC encodes location in a continuous or a categorical fashion[9–11], or even if working memory depends on a neural code based on persistent activity at all, or if it is better described by some slow transient dynamics[12–16]. Consistent with a continuous code, behavioral data shows a progressive spatial spread of inaccurate saccadic reports as the delay period is extended in spatial working memory tasks[2,17,18]. However, the possibility remains that PFC develops a discrete categorical representation after repeated training with a small number of visual cues and that a different mechanism related to elapsed time, not stimulus identity, is responsible for delay-dependent behavioral inaccuracies.

A unique feature of the bump attractor model for spatial working memory is that it predicts a particular relationship between neural activity and behavioral inaccuracies[2,17,18]. Given that the location of the bump of activity can vary continuously along the network, the bump is not constrained to remain centered at the same location in the absence of tuned external input during the delay period. Thus, the lack of sensory guidance during the delay makes the encoding vulnerable to random activity fluctuations. Although the shape of the bump is preserved by the network structure, the location of the center of the bump diffuses along the network[8,9,19–21]. This feature of the model has two important consequences: drifts of bump activity in PFC should be predictive of memory-dependent inaccuracies in the behavioral report of the remembered location, and this PFC neural dynamics should be reflected in a specific pattern of pairwise neuronal correlations[6,7,20].

We tested these predictions to examine the hypothesis that the bump attractor model is the neural substrate in PFC for spatial working memory. We scrutinized an experimental data set that includes single-neuron recordings, simultaneous neuron pair recordings and detailed behavioral data while monkeys performed a visuo-spatial delayed response task[3]. We tested four specific predictions of the bump attractor model. First, tuning curves computed on the basis of subsets of trials with disparate saccadic end points should show

[1]Institut d'Investigacions Biomèdiques August Pi i Sunyer, Barcelona, Spain. [2]School of Mathematics, University of Minnesota, Minneapolis, Minnesota, USA. [3]Wake Forest School of Medicine, Winston-Salem, North Carolina, USA. Correspondence should be addressed to A.C. (acompte@clinic.ub.es).

Received 25 November 2013; accepted 7 January 2014; published online 2 February 2014; doi:10.1038/nn.3645

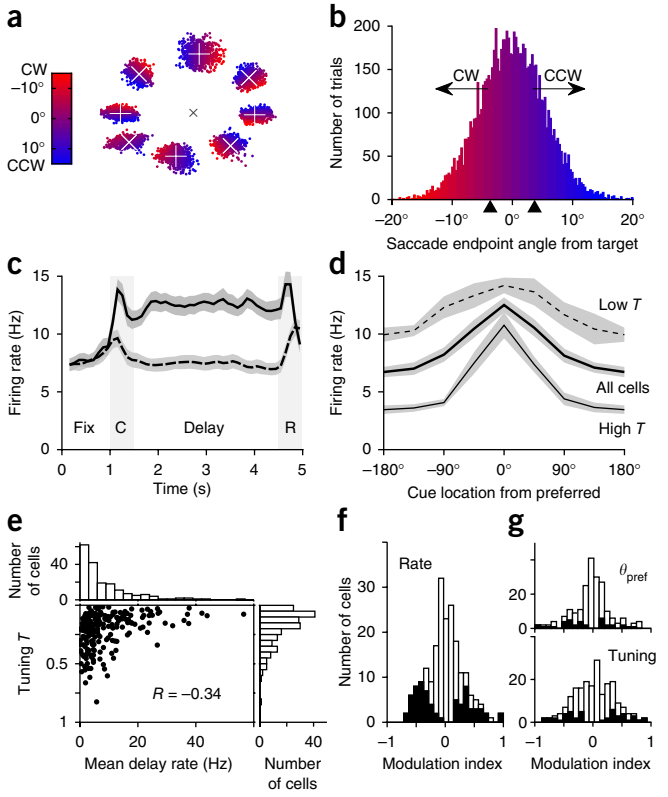

Figure 1 Behavioral and neural fingerprints of spatial working memory. (**a**) Saccade endpoints reporting cue location after a 3-s delay (fixation on black cross) for one monkey. White crosses indicate mean saccade locations for each of eight cues. Color indicates angular deviation from mean responses. CCW, counterclockwise; CW, clockwise. (**b**) Angular deviations pooled over cues and monkeys. Triangles indicate ± median absolute deviation. (**c**) PFC neurons represented cue location in selective sustained delay activity. Population activity (100-ms sliding window, $n = 204$) for preferred (solid) and non-preferred cues (dashed). Cue (C) and response (R) periods are marked in gray. (**d**) Population delay tuning curve for all neurons (thick line, $n = 204$) and for $n = 102$ neurons stronger (thin line) and weaker tuning (dashed line). (**e**) Distribution of mean delay firing rates (upper histogram, mean = 9 Hz, s.d. = 9.2 Hz), of tuning strength T (right histogram, mean = 0.21, s.d. = 0.15) and their correlation (central plot, $P < 0.0001$, $n = 204$). (**f**) Distribution of a rate modulation index (Online Methods) did not deviate significantly from a Gaussian (Lilliefors test, $P = 0.27$, $n = 204$) with zero mean (t test, $t = 0.23$, $P = 0.82$, $n = 204$). Negative (positive) values correspond to a firing rate decrease (increase) during the delay. Filled bars mark neurons with significant changes (Wilcoxon test, $P < 0.05$). (**g**) Distribution of modulation indexes for preferred location (top) and tuning strength T (bottom). Filled bars indicate neurons with significant changes (permutation test, $P < 0.05$). Gray shading shows bootstrap-estimated s.e.m.

a bias at the end of the delay period, before the monkey makes its response. Second, firing rate deviations should correlate positively with behavioral responses toward the neuron's preferred location, and this correlation should develop progressively through the delay. Third, neuronal variability right before saccade initiation should be higher for inaccurate than for accurate saccades. And finally, neuron pairs should be negatively correlated at the end of the delay, specifically for stimuli appearing between the two preferred locations[6,7,20]. In each case, our results supported the hypothesis that a bump attractor representation in the PFC maintains spatial information during working memory.

RESULTS

We trained two rhesus monkeys in an oculomotor spatial working memory task that required them to remember the spatial location of a brief (0.5 s) visual stimulus and execute a saccade toward the remembered location after a delay period of 3 s[3]. By tracking eye position, we collected a behavioral data set consisting of the coordinates of the saccadic end point for each successful trial in which the saccade correctly reported the approximate location of the memorized cue (**Fig. 1a** and Online Methods). For each monkey, we computed the mean saccadic end point for each of the eight cues presented. We computed a behavioral measure of accuracy as the angular distance on the screen from each trial's saccadic end point to the mean saccadic end point for the given cue. This measure classifies trials into clockwise and counterclockwise trials (**Fig. 1a**,**b**).

While the monkeys performed the task, we collected single-unit responses from the dorsolateral PFC. A substantial fraction of neurons in this area showed tuned persistent delay activity during the mnemonic phases of the task[2,3], and we selected these neurons for our further analyses ($n = 204$; **Fig. 1c**). We calculated memory tuning curves by averaging the delay period activity of each neuron across trials as a function of the eight equally spaced cues and determined a preferred cue angle (Online Methods). By aligning tuning curves by their preferred cue and averaging, we formed the population tuning curve (**Fig. 1d**).

On the other hand, individual neural responses were highly heterogeneous[22]. Mean firing rates during the delay period varied broadly across the population (**Fig. 1e**). Moreover, the degree of delay tuning to the cue varied widely among neurons. To quantify this, we calculated the tuning strength T for each neural tuning curve ($T = 0$ for non-tuned responses, $T = 1$ indicates response to one single cue; Online Methods). We found T to be broadly distributed (**Fig. 1e**). Mean firing rate and tuning strength were correlated across neurons (tuning curves for high T and low T neurons; **Fig. 1d**), with no clustering suggesting separate functional populations (**Fig. 1e**). Some neurons showed dynamics in their delay firing rate (**Fig. 1f**), with 30 of 204 (39 of 204) cells having significantly higher (lower) activity for preferred cues in the last compared with the first second of the delay (Wilcoxon test, $P < 0.05$). However, a majority of neurons (135 of 204) did not show a significant activity change, which was also the result for the population (Wilcoxon test, $P > 0.5$; **Fig. 1f**). Fano factors decreased slightly from the first to the last half of the delay period, from 1.29 ± 0.02 to 1.24 ± 0.03 (Wilcoxon test, $z = 3.6$, $P < 0.001$, $n = 196$). However, the tuning of individual neurons was markedly consistent through the delay period: preferred cue angles and tuning strength T did not change significantly between the first and last seconds of the delay (preferred angle: Harrison-Kanji test, $\chi^2 = 0.38$, $P = 0.8$; tuning T: Wilcoxon test, $z = -0.83$, $P = 0.4$, $n = 204$; **Fig. 1g**). The steadiness of the coding properties through the delay suggests that PFC activity can be described by a bump code, which could be responsible for behavioral performance during the task.

With this data, we tested the bump attractor hypothesis, the idea that trial-averaged memory tuning curves reflect a hill of population activity of invariant shape (bump attractor) that encodes during the delay period the information that will determine the upcoming saccade (**Fig. 2a**). The center of mass of the bump attractor can be at any position along a continuum and encodes a continuous representation of the visual cue's position. Random fluctuations in bump attractor position[6–8,21] lead to deviations in the read-out at the end of the delay, which result in inaccurate behavioral responses (**Fig. 2b**,**c**). This mechanism produces specific predictions regarding the

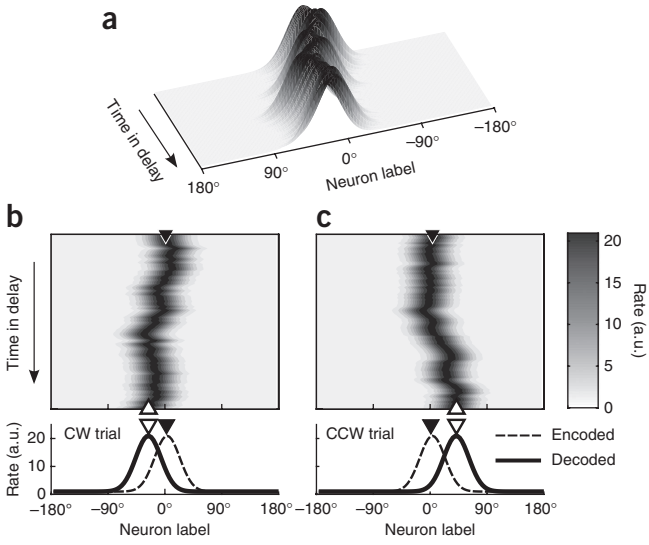

Figure 2 Bump attractor dynamics during the delay can explain behavioral inaccuracies. (**a**) Spatio-temporal representation of network activity during the delay period in an individual trial. Gray levels and *z* axis elevations schematize neuronal firing rates. (**b**) The same trial is presented as in **a**, but represented on the time-network plane. Gray scale represents firing rate elevations. The black triangle shows the location of the initial cue, right before the beginning of the delay (encoded population activity, bottom). The white triangle indicates the behavioral response decoded from network activity at the end of the delay (decoded population activity, bottom). Leftward displacement of the white relative to the black triangle indicates a clockwise behavioral response deviation in this trial. (**c**) Data are presented as in **b** but for a different trial. Rightward displacement of the white relative to the black triangle indicates a counterclockwise, inaccurate trial.

trial-to-trial relationship between variability in neural activity and variability in behavioral responses that we tested in the data.

Tuning-curve bias in the delay predicts behavioral biases

According to our hypothesis, population activity displacements at the end of the delay underlie behavioral response deviations. These displacements of population activity should be reflected in a systematic bias of delay tuning curves derived from the sets of trials that led to clockwise and counterclockwise deviations (**Supplementary Fig. 1**). For each neuron, we separated clockwise and counterclockwise trials for each cue condition (**Fig. 3a**) and computed the corresponding clockwise and counterclockwise tuning curves (**Fig. 3b**) as the corresponding trial-averaged firing rate versus the eight angles of the cue location. The tuning bias was defined as the signed angular distance from the counterclockwise to the clockwise tuning curve centers (Online Methods). With this definition, our hypothesis predicts that the tuning bias should become positive during the delay (**Supplementary Fig. 1**). We computed tuning biases for all neurons in different time windows along the trial and combined them to obtain the time evolution of the population tuning bias. Consistent with the bump attractor hypothesis, the population tuning bias became significantly positive at the end of the delay (tuning bias = 4.4 ± 2.9° in the last second of delay, one-sided permutation test, P = 0.024, n = 204), right before the behavioral response (**Fig. 3c**). To test for a possible motor origin of this signal, we repeated the analysis, excluding neurons with increasing rates in the delay period (positive modulation index; **Fig. 1f**), which have been shown to represent saccade preparation[23]. We still found significantly positive tuning bias in the last second of the delay (tuning bias = 9.9 ± 6.6°, one-sided permutation test, P = 0.014, n = 101), thereby excluding a driving role for saccade preparation neurons in generating the tuning bias during the delay.

In addition, we found a quantitative agreement between the mean tuning bias computed from our 204 neurons and the mean behavioral deviation computed as the difference between the average saccade end points of the corresponding counterclockwise and clockwise trials (mean tuning bias = 4.4 ± 2.9°, mean behavioral deviation = 7 ± 0.2°, Welch's test, t = 0.9, P = 0.36, n = 201). This order-of-magnitude match indicates that the bump attractor hypothesis in PFC can account for the magnitude of behavioral inaccuracies that we observed experimentally.

Correlation between delay activity and behavioral deviations

Thus, average tuning was related to dichotomized behavior (clockwise-counterclockwise; **Fig. 3**). In addition, the bump attractor model predicts that firing rates should correlate on a trial-by-trial basis with parametric deviations in behavioral response. In particular, a neuron increases its activity as the activity bump moves closer to its preferred location. As a result, trials for which a given neuron had stronger delay responses should result in behavioral deviations toward that neuron's preferred location. Thus, we would expect a positive correlation between firing rate and behavior attraction to the neuron's preferred location. This effect should be especially strong for neurons with strong tuning and for cues at the tuning curve flanks (that is, cues 1–2 positions from preferred), where responses are most sensitive to small variations in bump location (**Fig. 4**).

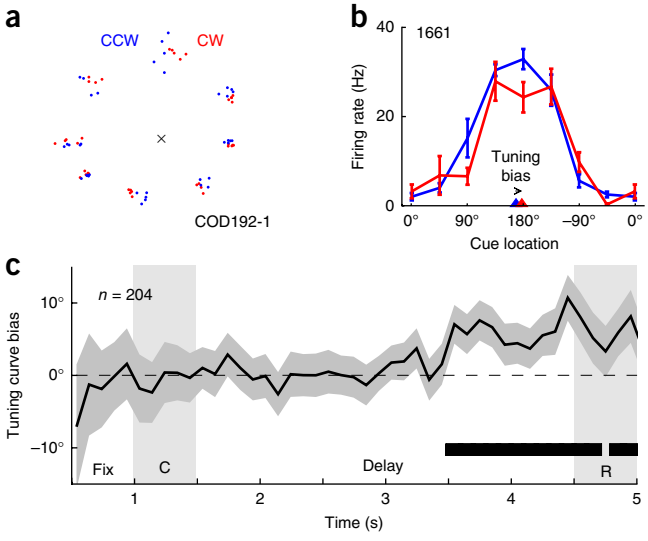

Figure 3 Tuning curves computed from clockwise and counterclockwise behavioral trials show model-predicted shift in the delay period. (**a**) Representation of saccade endpoints for one session. For each cue, trials are separated in half based on their relative clockwise (red) and counterclockwise (blue) saccadic responses. (**b**) Sample neuron delay-period responses in the clockwise and counterclockwise conditions. Triangles indicate the circular mean of the responses, an estimate of the preferred cue for each condition. The distance between these two circular means is the tuning bias. Error bars represent ±s.e.m. (**c**) Population average of the tuning bias for all neurons across time showed significantly positive values by the end of the delay (thick horizontal lines; permutation test, $P < 0.05$). Cue (C) and response (R) periods are indicated with gray areas. Tuning curves were estimated over 1-s sliding windows. Error bars (shaded area) indicate s.e.m.

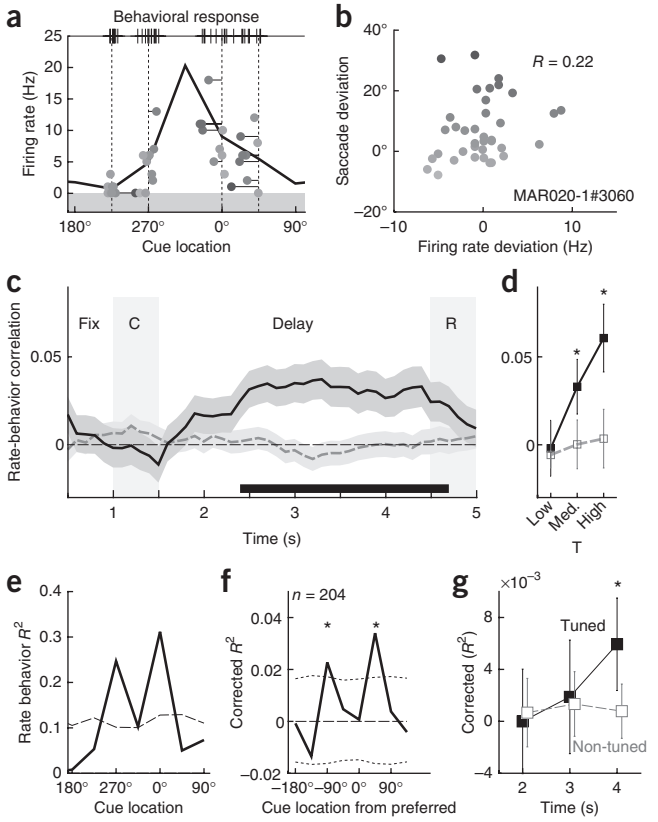

Figure 4 Responses to flank stimuli (1 and 2 locations from preferred) become correlated with upcoming behavior during the delay. (**a**) Sample neuron responses to flank stimuli superimposed on its tuning curve (data from last second of delay). Each circle represents a single trial: y is the neuron's firing rate and x is the angle of saccadic endpoint (also ticked on the line above). Dashed lines indicate cue locations and saccade deviations are marked with horizontal stems. Black (gray) circles indicate behavioral imprecision toward (away from) the neuron's preferred location. (**b**) Firing rate deviations from tuning curve correlate positively with saccadic deviations from cue location. Saccadic deviations toward the preferred cue have positive sign. The same data are presented as in **a.** (**c**) Population average of correlation coefficients computed as in **b** for tuned ($n = 204$, solid line) and non-tuned neurons ($n = 523$, dashed line). Rate-behavior correlations were computed over 1-s sliding windows. Shaded areas indicate bootstrapped s.e.m. Thick lines mark periods of significantly positive correlation (permutation test, $P < 0.05$). (**d**) Average rate-behavior correlation over the last 2 s of the delay for tuned (solid) and non-tuned neurons (dashed) with low, medium and high tuning strength T (**Supplementary Fig. 2**). (**e**) For the neuron shown in **a**, R^2 values for the linear regression of firing rate in the last 1 s of delay and behavioral deviations (solid line) were highest for individual flank stimuli. The dashed line is the mean R^2 for shuffled surrogates, $R^2_{shuffle}$. (**f**) Population average of corrected R^2 ($R^2 - R^2_{shuffle}$) was significantly positive for flank stimuli in tuned neurons ($P < 0.05$). Dashed lines are 95% confidence intervals for $R^2_{shuffled}$. (**g**) Corrected R^2 averaged over cues became significantly positive for tuned, but not non-tuned, neurons during the delay (late-delay tuned: $P = 0.045$, $n = 204$, one-tailed permutation test; 1-s non-overlapping windows). $^*P < 0.05$. Error bars represent ±s.e.m.

For each neuron, we selected the trials with stimuli in its tuning curve flanks (**Fig. 4a**) and matched the neuron's responses with the corresponding behavioral deviation (**Fig. 1b**). Defining behavioral deviations to be positive (negative) for saccades closer to (further from) the neuron's preferred location (**Fig. 4a**), we calculated the correlation coefficient between response deviation and behavioral deviation for each cell (**Fig. 4b**). We found that the population average of these correlations became positive during the delay period (**Fig. 4c**), especially for neurons with stronger tuning T (**Fig. 4d**). This effect persisted when removing neurons with ramping-up delay activity from the analysis (correlation in last second of delay = 0.029 ± 0.016, $P = 0.041$, $n = 101$, one-sided permutation test), thereby excluding saccade preparation as the cause of this signal.

This positive correlation accrued with time into delay (**Fig. 4c**), suggesting that behavioral deviations result from accumulated errors in prefrontal activity during the delay, as in our hypothesis (**Fig. 2**). We confirmed this by looking separately at cues at different distances from the preferred location (**Fig. 5**). If the bump were to diffuse during the delay (**Fig. 2**), the correlation between firing rate and behavior should appear earlier in trials in which the cue was presented closer to the cell's preferred location. This occurs because it takes more time for the bump to diffuse and modulate neurons with preferred locations more distant from the cue. Indeed, periods of significant correlation between neuronal and behavioral variability appeared later in the delay as we took flank cues more distant from preferred location (**Fig. 5**).

The trial-to-trial relationship between firing rate and behavior should be restricted to neurons participating in the bump. To test this, we investigated neurons without significant delay tuning

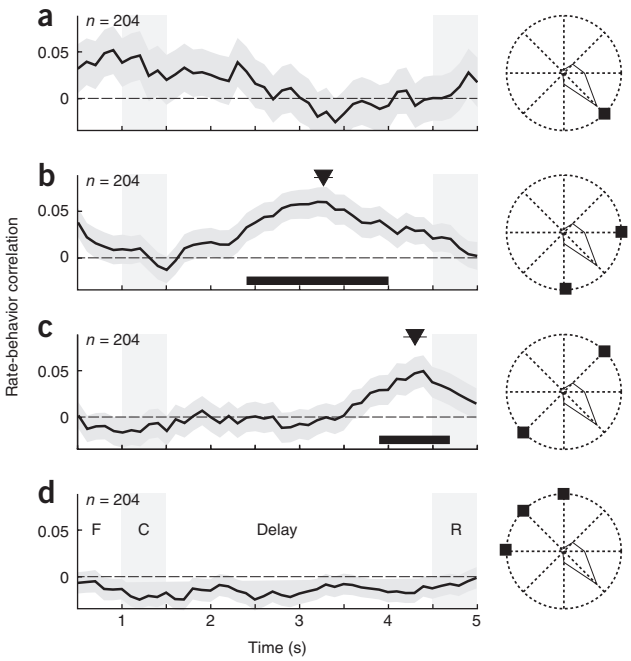

Figure 5 As predicted by the bump attractor model, neuronal variability correlates with upcoming behavioral responses in a cue-dependent way: maximally for flank stimuli and earlier in the delay for cues closer to the neuron's preferred location. (**a**) Absence of rate-behavior correlation for trials in which the presented cue coincided with the neuron's preferred location θ_{pref}. (**b**) Significant rate-behavior correlation (permutation test, $P < 0.05$), as early as 2 s before saccade, for trials with cues presented just next to θ_{pref}. (**c**) Late-delay rate-behavior correlation for cues presented two locations away from θ_{pref}. (**d**) Absence of rate-behavior correlation for cues opposing θ_{pref}. Correlation was computed in 1-s sliding windows. In **b** and **c** we evaluated the center of mass (black triangles) of time points with significantly positive correlation (one-sided permutation test, $P < 0.05$). Center of mass standard errors were evaluated with a bootstrap procedure. The curve shown in **Figure 4c** is the result of combining trials used in **b** and **c**. Error bars (shaded area) represent ±s.e.m.

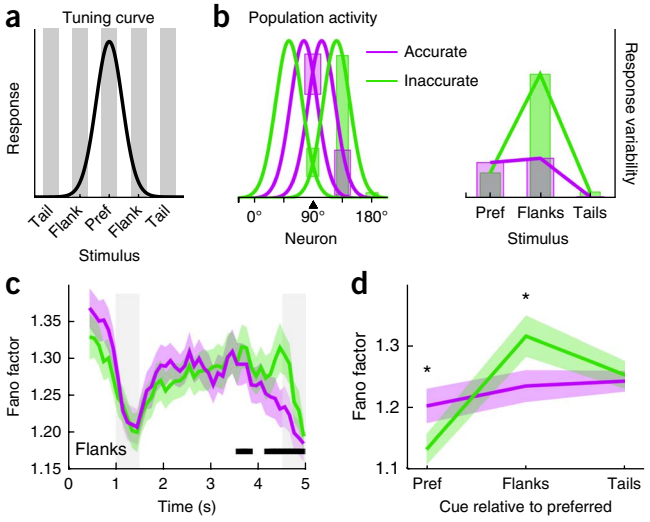

Figure 6 Fano factors follow the predictions of the bump attractor model. (**a**) Depending on the response properties of recorded neurons, cues can be classified as preferred, flank and tail cues. (**b**) Left, schematic representation of four different late-delay population activity profiles in response to the same 90° cue. Magenta lines represent trials with behavior closer to the target (accurate trials) and green lines trials with behavior farther from the target (inaccurate trials). The range of neural responses for these types of trials are marked with vertical rectangles for specific neurons in the network, those for which the presented cue represents a preferred, a flank or a tail cue. Right, according to the bump attractor hypothesis, neural response variability should be higher for inaccurate than accurate trials, selectively for flank stimuli. (**c**) In the data, when flank stimuli responses are separated into trials with behavioral responses farther or closer from the mean saccadic endpoint for that cue, Fano factor dynamics separate by the end of the delay with inaccurate responses showing higher Fano factors than accurate responses (one-sided permutation test, $P < 0.05$). (**d**) The difference between Fano factors in inaccurate and accurate trials at the end of the delay (averaging counts in the last 500 ms) depends on the cue condition. The Fano factor difference between accurate and inaccurate trials is significant for preferred and flank stimuli (*$P < 0.05$, permutation test, $n = 181$). Fano factor was computed in 100-ms windows. Error bars (shaded area) represent ±s.e.m.

(non-tuned neurons, $n = 523$; Online Methods and **Supplementary Fig. 2**). We found no significant correlation between responses to flank stimuli and behavioral deviations for this data set ($P > 0.05$; **Fig. 4c**,**d**). However, this analysis requires computing the preferred cue of each neuron, which probably suffered large estimation errors for such weakly tuned neurons. In addition, alignment to a preferred location could mask a rate-behavior relationship that is not related to the bump attractor hypothesis in these neurons. We therefore performed an additional analysis that did not assume a specific relationship between a neuron's tuning curve and behavioral deviations. For each neuron and each cue, we calculated the R^2 value of the linear regression between rate at the end of the delay and behavioral deviation (**Fig. 4e**). Consistent with the data shown in **Figure 4c**, the average of R^2 across tuned neurons was significant for two flank cues ($P < 0.05$; **Fig. 4f**). Crucially, the mean R^2 over all cues, averaged across all cells, became significant for tuned, but not non-tuned, neurons at the end of the delay ($P < 0.05$; **Fig. 4g**). Thus, non-tuned neurons did not show a detectable rate-behavior relationship in our data set.

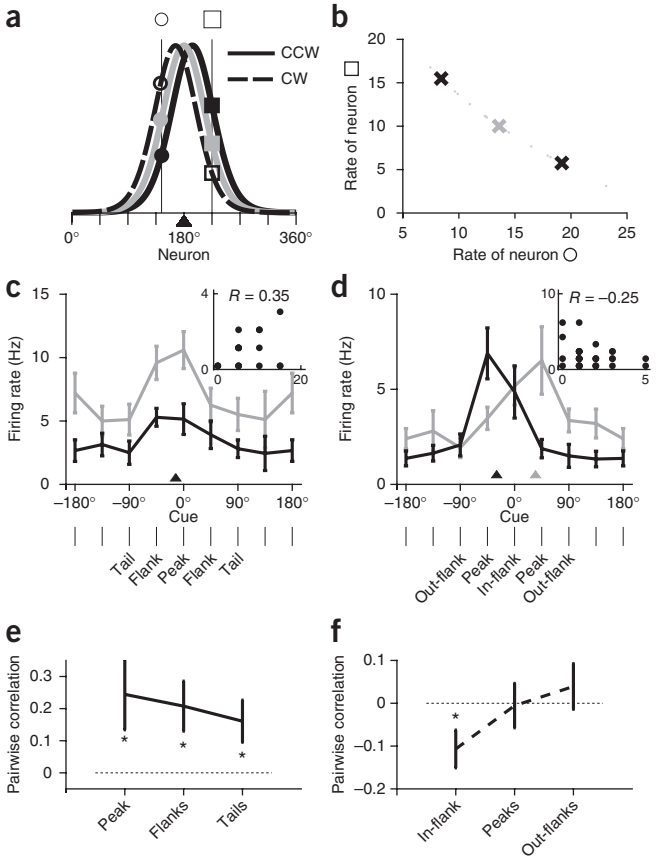

Late-delay behavioral modulations of Fano factors

We then tested the contribution of bump attractor diffusion to neuronal variability, as captured by the Fano factor. Following our hypothesis, bump displacements in different trials induced behavioral inaccuracies and led to the largest variation in neuronal response for cues in the flanks of a neuron's tuning curve (**Fig. 6a**,**b**). For these cues, random diffusion of the bump caused maximal neuronal activation in trials in which the bump drifted toward the neuron's preferred location, and minimal activation when it drifted away (**Fig. 6b**). Our hypothesis predicts that the variance of neural responses to flank stimuli should be larger for trials with inaccurate compared with more accurate behavior. Moreover, this difference should be specific to flank stimuli and absent, or even inverted, for preferred or tail

Figure 7 Noise correlations between pairs of neurons depend on the stimulus as predicted by the bump attractor model. (**a**) Scheme of delay population activity profiles in response to three repeated presentations of 180° cue. We focus on two neurons in this schematic network (○ and □) lying at opposite sides of the activity bump. (**b**) Only in this configuration, trial-to-trial correlations between the two neurons are expected to be negative because a displacement of the bump, illustrated in **a**, leads to an increase of firing rate in one neuron and a decrease in the other neuron (○ and □ in **a**). (**c**) Delay-period tuning curves for a sample pair of PFC neurons with the same preferred cue. Relevant cue conditions are indicated below the *x* axis. Spike count correlations were computed for each pair in the final 200 ms of the delay. Inset, scatter plot of spike counts for this sample pair. (**d**) Data presented as in **c** for a pair of neurons whose preferred cues were separated by one cue. Inset, scatter plot of spike counts for the 'in-flank' stimulus. (**e**) Pairwise correlation for same-tuning pairs ($n = 15$) computed separately for peak, flank and tail cue conditions. Significant deviation from zero mean was tested combining the last two 200-ms bins in the delay period (two-tailed *t* test, $P < 0.05$, $n = 30$). (**f**) Data presented as in **e** for different-tuning pairs ($n = 10$). Negative correlation for in-flank stimuli was tested with one-sided *t* test ($t = 2.42$, $P = 0.026$, $n = 20$). *$P < 0.05$. Error bars represent ±s.e.m.

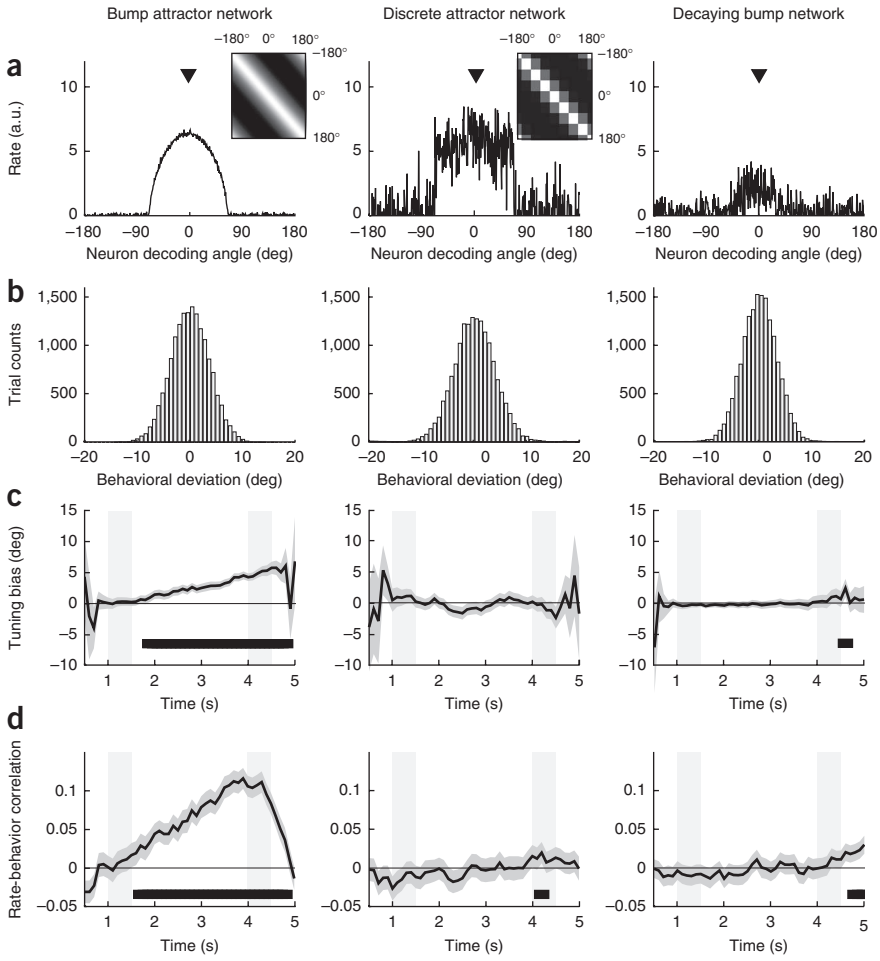

Figure 8 Comparison of three alternative memory representations in three mechanistic models: a bump attractor model maintained by continuous topographic recurrent excitation (left), a discrete attractor model with eight populations (middle) and a non-attractor decaying bump model sustained by a slow intrinsic current (right). (**a**) Sample simulated delay activity in one trial for each model (see **Supplementary Videos 1–3**). Triangles mark decoded response. Insets display recurrent excitatory connectivity patterns. (**b**) Distributions of behavioral responses over 16,000 simulations for each model reveal similar behavioral variability. (**c**) Tuning bias analysis as in **Figure 3** for neural and behavioral data obtained from each model revealed significant positive bias only for the bump attractor model (thick horizontal lines; permutation test, $P < 0.05$). (**d**) Correlation between rate and behavioral deviations toward the neuron's preferred location (as in **Fig. 4**) becomes gradually positive in the delay only for the bump attractor model. Error bars (shaded area) represent ±s.e.m.

stimuli (**Fig. 6b**). Note that the variance of neural responses is also affected by independent spiking noise, typically in proportion to the mean response[24,25]. This contribution will not interfere qualitatively with our prediction, assuming its invariance across task conditions[25].

We separated inaccurate trials, in which the monkey made saccadic responses beyond the median absolute angular displacement (**Fig. 1b**), from accurate trials, which contained the same number of trials for each neuron and cue combination as the inaccurate group, but with the smallest angular displacement. In flank-cue trials, the Fano factor for accurate and inaccurate trials differed significantly at the end of the delay period, as predicted (last 0.5 s of delay, one-sided paired t test, $t = 1.56$, $P = 0.05$, $n = 181$; **Fig. 6c**). This difference increased parametrically as we restricted inaccurate trials to the most extreme saccadic deviations (**Supplementary Fig. 3**). The effect was specific for flank stimuli (**Fig. 6d**): modeling Fano factor with a mixed-effects ANOVA with factors cue, accuracy, monkey and neuron identity as random factor yielded a significant interaction effect of cue × accuracy ($F_{2,897} = 6.69$, $P = 0.0013$, cell size 152 or 29 depending on monkey; **Supplementary Fig. 4**). Reduced ANOVA models revealed a main effect of cue for inaccurate trials ($F_{2,360} = 16.01$, $P < 0.001$) and no significant cue effect for accurate trials ($F_{2,360} = 1.32$, $P = 0.27$).

Late delay–selective negative pairwise correlations

We finally tested a long-standing prediction on how spike count correlations between neurons depend on the neurons' tuning preferences and the cue in a bump attractor representation[6,7,20]. We expected negative trial-to-trial correlations in the delay activity of two neurons responding to a cue presented right between their two preferred locations, resulting from random bump displacements in different trials (**Fig. 7a,b**). Only for this condition, when the cue engages the neurons in parts of their tuning curve with slopes of opposite sign, would we expect a negative correlation. Other cue conditions or correlations for neurons with the same selectivity should show positive or vanishing correlations[6,7].

We selected neuron pairs in two conditions: same-tuning pairs, with neurons sharing preferred cue ($n = 15$; **Fig. 7c**), and different-tuning pairs, where neurons differed in preferred location with one intervening cue in between ($n = 10$; **Fig. 7d**). We computed correlations between responses in the pair (**Fig. 7c,d**) for various cue conditions (peak, flank and tail, and in-flank, peak and out-flank; **Fig. 7c,d**) both in early and late delay (200-ms windows). Same-tuning pairs had stronger correlations than different-tuning pairs (three-way ANOVA with factors time, cue and neuron selectivity difference: main effect of selectivity difference, $F_{1,272} = 25.6$, $P < 0.001$; no interaction effects, $P > 0.2$; **Supplementary Fig. 4e–h**). In same-tuning pairs, no other interaction or main effect was significant (factorial ANOVA, factors time and cue, $P > 0.5$), indicating consistently positive correlations through the delay, independently of the cue (**Fig. 7e**). Instead, a significant interaction of time and cue emerged for different-tuning pairs ($F_{2,114} = 3$, $P = 0.05$), which reflected pairwise correlations becoming significantly negative at the end of the delay for in-flank stimuli (**Fig. 7f**). Thus, spike count correlations changed with cue condition as predicted by the bump attractor hypothesis.

The data can distinguish alternative scenarios

To test the extent to which our experimental data could distinguish the bump attractor model from other alternative encoding hypotheses for memory maintenance in PFC, we formulated two alternative models, the discrete attractor and the decaying bump network models (**Supplementary Videos 1–3**). The continuous bump attractor network features strong topographic connectivity between excitatory

neurons, so that a rigid bump attractor stabilized after brief network activation and diffused in the network during the delay period as a result of external noisy inputs (**Fig. 8a**). The discrete attractor network includes eight populations, each one encoding one of the cue locations, with stronger connections within and weaker connections across populations. An external stimulus brought the system to an attractor that maintained three adjacent populations persistently active and subject to strong external noise (**Fig. 8a**). Finally, in the decaying bump network, mnemonic information is encoded by individual neurons through an intrinsic depolarizing current that slowly decays away after initial activation by the stimulus. The bump of activity therefore slowly decayed away during the delay period (**Fig. 8a**).

To test whether a neural data set with the characteristics of our experimental data can distinguish between these models, we performed simulations with the three firing rate models (Online Methods and **Supplementary Codes 1–3**), and we generated three surrogate data sets matching the sample sizes in our experiment. We picked parameters for our models that produced similar neural and behavioral data (**Fig. 8a**,**b**), in good qualitative agreement with experimental data (**Fig. 1**). To get a sense of the quantitative effects expected, we also tested non-mechanistic coding models that could match quantitatively the heterogeneity of experimental neural data (Online Methods and **Supplementary Figs. 5** and **6**).

We analyzed these surrogate data sets exactly as we did before for the experimental data. Data produced by the bump attractor model replicated our experimental findings, but none of the effects were replicated by the discrete attractor or the decaying bump models (tuning curve bias, rate-behavior correlation, Fano factor and pairwise correlations; **Fig. 8c**,**d** and **Supplementary Fig. 6**). For these models, the lack of effects occurred because behavioral variability did not result primarily from collective neuronal variability: both in the discrete attractor and in the decaying bump models behavioral variability emerged largely from independent random fluctuations at the cellular level, and not from correlated population dynamics as in the bump attractor model. Such dynamics can occur in discrete attractor models, in the form of noise-induced transitions to adjacent attractors. However, this leads to large abrupt shifts in behavioral read-out, which result in multimodal behavioral distributions, that were not supported experimentally (**Fig. 1b**) unless very fine discretization approaching a continuum is assumed. We conclude that our experimental findings can discriminate between distinct mechanisms of working memory maintenance, supporting a neural representation in PFC compatible with the bump attractor hypothesis for spatial working memory.

DISCUSSION

We analyzed behavioral and electrophysiological data from monkeys performing a spatial working memory task and tested predictions from an attractor bump hypothesis for spatial memory maintenance. Our analyses confirm the model predictions, supporting the hypothesis that PFC activity represents spatial memories in a fixed-shape bump of activity that is used for guiding behavior, but is liable to cumulative encoding errors as a result of random fluctuations. Our results affect our conceptual understanding of PFC activity in spatial working memory by validating the concept of prefrontal persistent activity as the basis of spatial working memory, supporting the continuous (or finely discretized) nature of spatial memory encoding in PFC, and being consistent with bump attractor dynamics mediating cognitive function in the cortex.

The concept of persistent activity has been highly influential in formulating concrete mechanistic models for working memory[10,19,26,27], but it cannot account naturally for the great heterogeneity, irregularity and dynamics of prefrontal activity during delayed response tasks[9,14–16,28–31]. Recent studies have shown that biophysical neural network mechanisms for persistent activity can accommodate heterogeneity in firing rates and tuning properties[32,33], as well as irregular spiking activity[33,34]. In addition, variable neural activity in the delay period after identical stimulus presentation can reflect insufficient conditioning to details of sensory stimuli or behavior. According to this view, variability in the delay period should be predictive of behavioral responses. Our data confirms this for PFC neural variability in spatial working memory tasks, consistent with choice probability measurements in other cognitive tasks[28,35]. Finally, heterogeneity might reflect the presence of distinct functional populations[36]. Consistent with this, we found a significant relationship between trial-to-trial variability of neuronal responses and the fine details of behavioral reports for neurons with sustained and tuned delay activity, but not for non-tuned neurons (**Fig. 4**).

Non-stationary responses are more difficult to account for in attractor network models of working memory[9]. Alternative neural mechanisms have been proposed that rely on sequential activation of neuronal subpopulations[13] or storage in short-term synaptic states[12], rather than on sustained neural spiking. It is unclear how these alternative models could accommodate our experimental findings. Here, we discarded a non-attractor model based on the slow decay of an initial bump of activity, although the data was still consistent with a diffusing bump representation that also undergoes slow decay. However, we cannot rule out that other non-attractor models may explain some of our findings. Testing this would require building spatial working memory networks based on these other theoretical frameworks.

In addition, several independent dynamical components may converge in shaping neural activity in PFC[37]. In our task, a timing component related to the predictability of task events could partly explain some temporal dynamics observed in Fano factors or firing rates, whereas a stimulus encoding component would determine neural tuning. The assumption that these components are independent[37] is implicit in our Fano factor analysis (**Fig. 6**), where we did not pay attention to temporal dynamics and instead focused on neural tuning and behavior. A related concern is that a tuned ramping-up component related to motor parameters, known to emerge in late delay[23], may dominate our results, thereby reflecting saccade preparation and not working memory in PFC. We have ruled out this possibility by showing that our results persist when excluding neurons with ramping-up delay activity from the analyses.

Our results support a continuous or finely discretized spatial encoding of memorized locations in the PFC. This is remarkable because our two monkeys were tested over the course of 1 year in a task that involved the same eight identical cues, at specific locations in their visual space. This could have generated a neural code that emphasized these eight discrete locations without much selectivity for intermediate positions[38] (discrete attractor model; **Fig. 8**). Such task-tailored representation during working memory delays has been seen in the PFC for other types of task requirements[39]. Our findings set apart spatial working memory in this respect, suggesting that a continuous representation for memorized space is permanently present in PFC, possibly reinforced by everyday navigation in a spatially continuous environment. This is consistent with evidence showing that prefrontal neurons have mnemonic spatial fields even in untrained animals[40].

Noise correlations are known to depend on tuning curve similarity (that is, on signal correlations)[41–43], but the extent to which they depend on the stimulus remains unclear[41,42,44]. We found that noise

correlations between PFC neurons depended on the location of the memorized stimulus. This is further evidence that noise correlations do not just reflect fixed hard-wired connectivity, but instead reflect network dynamics and ongoing computations, such as attentional[45] and context-depending processing[43]. Moreover, we found negative noise correlations in very specific stimulus conditions (**Fig. 7**), confirming a long-standing prediction of bump attractor models[6,7]. This finding is in contrast with another study[41], which did not find evidence for negative stimulus–induced correlations in orientation-tuned neurons in primary visual cortex (V1) of anesthetized monkeys. Different network dynamics in PFC and V1, and/or different brain states, in awake versus anesthetized animals could be responsible for this difference.

Experimental studies searching for evidence of attractor dynamics in neural activity during behavior have focused on testing whether neuronal spiking converges to discrete singular patterns following parametric changes in sensory stimuli[46–48], following changes in reward rules[49] or during distinct phases of a multi-component cognitive task[50]. These approaches can identify dynamics governed by discrete attractors, where small changes in task conditions shift the neural representation abruptly to a new attractive state. However, they cannot identify continuous attractors, such as the bump attractor, as such attractors have one continuous dimension and one therefore does not expect abrupt changes to small modifications of external conditions. Our findings demonstrate that identifying the behavioral parameters associated with the direction of marginal stability in the model, here the small angular inaccuracies in behavioral report, can provide model-dependent tests to apply to the data and validate a continuous attractor explanation for the underlying neural dynamics. Our results implicate a bump attractor code in the PFC mediating the precision of response in spatial working memory.

METHODS

Methods and any associated references are available in the online version of the paper.

Note: Any Supplementary Information and Source Data files are available in the online version of the paper.

ACKNOWLEDGMENTS

We thank M. Goldman, J. de la Rocha and A. Roxin for fruitful discussions. We wish to acknowledge the late P. Goldman-Rakic, in whose laboratory experimental data were collected. This work was funded by the Ministry of Economy and Competitiveness of Spain, the European Regional Development Fund (Ref: BFU2009-09537) and by the National Science Foundation (NSF PHY11-25915 and DMS-0847749). K.W. acknowledges funding from the German Research Foundation (research fellowship Wi 3767/1-1). D.Q.N. was supported by the Generalitat de Catalunya (PIV-DGR 2010 program). C.C. received support from the Tab Williams Family Endowment. The work was carried out at the Esther Koplowitz Centre and partly at the Kavli Institute for Theoretical Physics, and at the Centre de Recerca Matemàtica.

AUTHOR CONTRIBUTIONS

A.C. conceived and designed the study. C.C. collected the experimental data. K.W. and A.C. analyzed the data. D.Q.N. and A.C. implemented the computational models. A.C., C.C., D.Q.N. and K.W. wrote the manuscript.

COMPETING FINANCIAL INTERESTS

The authors declare no competing financial interests.

1. Gnadt, J.W. & Andersen, R.A. Memory related motor planning activity in posterior parietal cortex of macaque. *Exp. Brain Res.* **70**, 216–220 (1988).
2. Funahashi, S., Bruce, C.J. & Goldman-Rakic, P.S. Mnemonic coding of visual space in the monkey's dorsolateral prefrontal cortex. *J. Neurophysiol.* **61**, 331–349 (1989).
3. Constantinidis, C., Franowicz, M.N. & Goldman-Rakic, P.S. Coding specificity in cortical microcircuits: a multiple-electrode analysis of primate prefrontal cortex. *J. Neurosci.* **21**, 3646–3655 (2001).
4. Wilson, H.R. & Cowan, J.D. A mathematical theory of the functional dynamics of cortical and thalamic nervous tissue. *Kybernetik* **13**, 55–80 (1973).
5. Amari, S. Dynamics of pattern formation in lateral-inhibition type neural fields. *Biol. Cybern.* **27**, 77–87 (1977).
6. Ben-Yishai, R., Bar-Or, R.L. & Sompolinsky, H. Theory of orientation tuning in visual cortex. *Proc. Natl. Acad. Sci. USA* **92**, 3844–3848 (1995).
7. Pouget, A., Zhang, K., Deneve, S. & Latham, P.E. Statistically efficient estimation using population coding. *Neural Comput.* **10**, 373–401 (1998).
8. Compte, A., Brunel, N., Goldman-Rakic, P.S. & Wang, X.J. Synaptic mechanisms and network dynamics underlying spatial working memory in a cortical network model. *Cereb. Cortex* **10**, 910–923 (2000).
9. Brody, C.D., Romo, R. & Kepecs, A. Basic mechanisms for graded persistent activity: discrete attractors, continuous attractors and dynamic representations. *Curr. Opin. Neurobiol.* **13**, 204–211 (2003).
10. Constantinidis, C. & Wang, X.-J. A neural circuit basis for spatial working memory. *Neuroscientist* **10**, 553–565 (2004).
11. Miller, P. Analysis of spike statistics in neuronal systems with continuous attractors or multiple, discrete attractor states. *Neural Comput.* **18**, 1268–1317 (2006).
12. Mongillo, G., Barak, O. & Tsodyks, M. Synaptic theory of working memory. *Science* **319**, 1543–1546 (2008).
13. Goldman, M.S. Memory without feedback in a neural network. *Neuron* **61**, 621–634 (2009).
14. Barak, O., Tsodyks, M. & Romo, R. Neuronal population coding of parametric working memory. *J. Neurosci.* **30**, 9424–9430 (2010).
15. Jun, J.K. *et al.* Heterogenous population coding of a short-term memory and decision task. *J. Neurosci.* **30**, 916–929 (2010).
16. Hussar, C.R. & Pasternak, T. Memory-guided sensory comparisons in the prefrontal cortex: contribution of putative pyramidal cells and interneurons. *J. Neurosci.* **32**, 2747–2761 (2012).
17. White, J.M., Sparks, D.L. & Stanford, T.R. Saccades to remembered target locations: an analysis of systematic and variable errors. *Vision Res.* **34**, 79–92 (1994).
18. Ploner, C.J., Gaymard, B., Rivaud, S., Agid, Y. & Pierrot-Deseilligny, C. Temporal limits of spatial working memory in humans. *Eur. J. Neurosci.* **10**, 794–797 (1998).
19. Wang, X.J. Synaptic reverberation underlying mnemonic persistent activity. *Trends Neurosci.* **24**, 455–463 (2001).
20. Wu, S., Hamaguchi, K. & Amari, S. Dynamics and computation of continuous attractors. *Neural Comput.* **20**, 994–1025 (2008).
21. Burak, Y. & Fiete, I.R. Fundamental limits on persistent activity in networks of noisy neurons. *Proc. Natl. Acad. Sci. USA* **109**, 17645–17650 (2012).
22. Shafi, M. *et al.* Variability in neuronal activity in primate cortex during working memory tasks. *Neuroscience* **146**, 1082–1108 (2007).
23. Constantinidis, C., Franowicz, M.N. & Goldman-Rakic, P.S. The sensory nature of mnemonic representation in the primate prefrontal cortex. *Nat. Neurosci.* **4**, 311–316 (2001).
24. Shadlen, M.N. & Newsome, W.T. The variable discharge of cortical neurons: implications for connectivity, computation and information coding. *J. Neurosci.* **18**, 3870–3896 (1998).
25. Churchland, A.K. *et al.* Variance as a signature of neural computations during decision making. *Neuron* **69**, 818–831 (2011).
26. Goldman-Rakic, P.S. Cellular basis of working memory. *Neuron* **14**, 477–485 (1995).
27. Durstewitz, D., Seamans, J.K. & Sejnowski, T.J. Neurocomputational models of working memory. *Nat. Neurosci.* **3**, 1184–1191 (2000).
28. Brody, C.D., Hernández, A., Zainos, A. & Romo, R. Timing and neural encoding of somatosensory parametric working memory in macaque prefrontal cortex. *Cereb. Cortex* **13**, 1196–1207 (2003).
29. Zaksas, D. & Pasternak, T. Directional signals in the prefrontal cortex and in area MT during a working memory for visual motion task. *J. Neurosci.* **26**, 11726–11742 (2006).
30. Meyers, E.M., Freedman, D.J., Kreiman, G., Miller, E.K. & Poggio, T. Dynamic population coding of category information in inferior temporal and prefrontal cortex. *J. Neurophysiol.* **100**, 1407–1419 (2008).
31. Compte, A. *et al.* Temporally irregular mnemonic persistent activity in prefrontal neurons of monkeys during a delayed response task. *J. Neurophysiol.* **90**, 3441–3454 (2003).
32. Renart, A., Song, P. & Wang, X.-J. Robust spatial working memory through homeostatic synaptic scaling in heterogeneous cortical networks. *Neuron* **38**, 473–485 (2003).
33. Hansel, D. & Mato, G. Short-term plasticity explains irregular persistent activity in working memory tasks. *J. Neurosci.* **33**, 133–149 (2013).
34. Barbieri, F. & Brunel, N. Irregular persistent activity induced by synaptic excitatory feedback. *Front. Comput. Neurosci.* **1**, 5 (2007).
35. Britten, K.H., Newsome, W.T., Shadlen, M.N., Celebrini, S. & Movshon, J.A. A relationship between behavioral choice and the visual responses of neurons in macaque MT. *Vis. Neurosci.* **13**, 87–100 (1996).

36. Jun, J.K. *et al.* Heterogeneous population coding of a short-term memory and decision task. *J. Neurosci.* **30**, 916–929 (2010).
37. Machens, C.K., Romo, R. & Brody, C.D. Functional, but not anatomical, separation of 'what' and 'when' in prefrontal cortex. *J. Neurosci.* **30**, 350–360 (2010).
38. Kilpatrick, Z.P., Ermentrout, B. & Doiron, B. Optimizing working memory with heterogeneity of recurrent cortical excitation. *J. Neurosci.* **33**, 18999–19011 (2013).
39. Miller, E.K. The prefrontal cortex and cognitive control. *Nat. Rev. Neurosci.* **1**, 59–65 (2000).
40. Meyer, T., Qi, X.-L. & Constantinidis, C. Persistent discharges in the prefrontal cortex of monkeys naive to working memory tasks. *Cereb. Cortex* **17**, i70–i76 (2007).
41. Kohn, A. & Smith, M.A. Stimulus dependence of neuronal correlation in primary visual cortex of the macaque. *J. Neurosci.* **25**, 3661–3673 (2005).
42. Bair, W., Zohary, E. & Newsome, W.T. Correlated firing in macaque visual area MT: time scales and relationship to behavior. *J. Neurosci.* **21**, 1676–1697 (2001).
43. Cohen, M.R. & Newsome, W.T. Context-dependent changes in functional circuitry in visual area MT. *Neuron* **60**, 162–173 (2008).
44. Ponce-Alvarez, A., Thiele, A., Albright, T.D., Stoner, G.R. & Deco, G. Stimulus-dependent variability and noise correlations in cortical MT neurons. *Proc. Natl. Acad. Sci. USA* **110**, 13162–13167 (2013).
45. Mitchell, J.F., Sundberg, K.A. & Reynolds, J.H. Spatial attention decorrelates intrinsic activity fluctuations in macaque area V4. *Neuron* **63**, 879–888 (2009).
46. Amit, D.J., Fusi, S. & Yakovlev, V. Paradigmatic working memory (attractor) cell in IT cortex. *Neural Comput.* **9**, 1071–1092 (1997).
47. Leutgeb, J.K. *et al.* Progressive transformation of hippocampal neuronal representations in 'morphed' environments. *Neuron* **48**, 345–358 (2005).
48. Wills, T.J., Lever, C., Cacucci, F., Burgess, N. & O'Keefe, J. Attractor dynamics in the hippocampal representation of the local environment. *Science* **308**, 873–876 (2005).
49. Durstewitz, D., Vittoz, N.M., Floresco, S.B. & Seamans, J.K. Abrupt transitions between prefrontal neural ensemble states accompany behavioral transitions during rule learning. *Neuron* **66**, 438–448 (2010).
50. Balaguer-Ballester, E., Lapish, C.C., Seamans, J.K. & Durstewitz, D. Attracting dynamics of frontal cortex ensembles during memory-guided decision-making. *PLoS Comput. Biol.* **7**, e1002057 (2011).

ONLINE METHODS

Behavioral task and recordings. Two adult, male rhesus monkeys (*Macaca mulatta*) were trained in an oculomotor delayed response task requiring them to view a visual stimulus on a screen and make an eye movement after a delay period. During execution of the task, neurophysiological recordings were obtained from the lateral prefrontal cortex. Detailed methods of the behavioral task, training, surgeries and recordings, as well as descriptions of neuronal responses in the task have been published previously[3,31,51,52] and are only summarized briefly here. Visual stimuli were 1° squares, flashed for 500 ms at an eccentricity of 14°. Stimuli were presented randomly at one of 8 possible locations around the fixation point. A delay period lasting 3 s followed the presentation of the stimulus, at the end of which the fixation point turned off, and an eye movement toward the location of the remembered stimulus was reinforced with liquid reward. Eye position was monitored with a scleral eye coil system. Neuronal activity was monitored using tungsten electrodes of 1–4-MΩ impedance at 1 kHz. All experiments were conducted in accordance with the guidelines set forth by the US National Institutes of Health, as reviewed and approved by the Yale University Institutional Animal Care and Use Committee.

Data analysis. A total of 822 neurons were recorded from two monkeys with the eight-target oculomotor delayed response task. Sample size was determined by the fact that it had been collected previously[3,31,51,52]. Neuronal responses in this task have been characterized previously[3], but their trial-to-trial relationship to behavioral parameters has not been investigated before. We compiled our data set with neurons that showed significant tuned delay period activity, evaluated using a bootstrap method as explained in ref. 3 and for which end points of saccadic eye movements were available. Our database thus consisted of 204 tuned neurons, 172 from monkey COD and 32 from monkey MAR. For some analyses in **Figure 4**, we also compiled a data set with the remaining neurons that did not show significant tuned delay activity and for which behavioral response data was available (non-tuned neurons, n = 523: 388 from monkey COD and 135 from monkey MAR).

In parallel, we built an additional database with pairs of neurons recorded simultaneously, from the same or separate electrodes 0.2–1 mm apart, both of which showed tuned delay activity as per the criteria described above. This database consisted of n = 64 pairs, 53 of which were recorded in monkey COD and 11 of which came from monkey MAR. All of our results subsisted if we eliminated pairs recorded from the same electrode from our correlation analyses (7 of 15 same-selectivity pairs, and 2 of 10 different-selectivity pairs came from a single electrode). This affected especially the power of the statistical tests concerning same-selectivity pairs (**Fig. 7e**), but none of the essential effects reported here.

For each neuron in our database, preferred location was determined by computing the circular mean of the cue angles (0° to 315°, in steps of 45°) weighted by the neuron's mean spike count over the delay period (3 s) following each cue presentation. To this end, we computed for each neuron the complex quantity

$$\mathbf{T} = \left(\sum_{j=1}^{8} n_j e^{i\theta_j}\right)\left(\sum_{j=1}^{8} n_j\right)^{-1}$$

where n_j is the mean spike count during the delay period in response to the cue θ_j (j = 1…8), and we extracted its modulus T and angle θ_{pref}: $\mathbf{T} = Te^{i\theta_{\text{pref}}}$. The angle θ_{pref} constitutes our estimate of the neuron's preferred location during the delay, and the tuning strength T is our estimate of the delay tuning quality. T can reach a maximal value of 1 when the neuron responds exclusively to one cue during the delay (that is, $n_j = 0$ for all $\theta_j \neq \theta_{\text{pref}}$) and a minimum value of 0 when the neuron's response is evenly balanced around the circle, such as the case when the neuron responds with equal number of spikes to all cues (all n_j equal).

Spike trains for each neuron and condition (cue in one of eight possible locations) were analyzed in time windows of various lengths (typically 1 s for tuning curve and firing rate estimations, 0.1 s for Fano factor estimations, 0.2 s for spike count correlations) that slid over the duration of the trial in steps of 0.1 s to estimate trial-related time evolution. To test stationarity through the delay we computed modulation indices for preferred rate and tuning as the difference in measures obtained in the first and last second of the delay divided by their sum (**Fig. 1f**,**g**). The modulation index for preferred location θ_{pref} (**Fig. 1g**) was computed as the circular distance between θ_{pref} estimated in the first and last seconds of the delay, divided by the maximal possible distance of 180°. All these modulation indices share the property that they are bounded between –1 and 1 and stationarity is characterized by a concentration around 0.

Displacements of tuning curves computed for clockwise (CW) and counterclockwise (CCW) behavior trials (**Fig. 3**) were evaluated with the tuning bias. We defined this tuning bias as $\theta_{\text{pref}}^{\text{CW}} - \theta_{\text{pref}}^{\text{CCW}}$, where $\theta_{\text{pref}}^{\text{CW}}$ $\left(\theta_{\text{pref}}^{\text{CCW}}\right)$ is the neuron's preferred location calculated as detailed above but restricting it to clockwise (counterclockwise) behavior trials (see **Fig. 3a**). Notice that a positive value of the tuning bias results when the preferred location for clockwise trials is displaced counterclockwise relative to the preferred location for counterclockwise trials. A positive tuning bias is expected for tuning curves generated from displaced population activity bumps (**Supplementary Fig. 1**), as described in previous computational studies[53,54]. Thus, the bump attractor hypothesis predicts a significantly positive tuning bias $\theta_{\text{pref}}^{\text{CW}} - \theta_{\text{pref}}^{\text{CCW}}$ at the end of the delay period. Given that this analysis depends on the estimation of two centers of tuning curves, each derived from half the typical number of trials, we expect the tuning bias to be better estimated in well-tuned neurons. To emphasize the tuning properties of neurons with better tuning, we computed the population tuning bias as an average weighted by our tuning measure T.

The population Fano factor was estimated as

$$FF = \frac{N_T^{-1}\sum N_i FF_i}{N_T^{-1}\sum N_i} = \langle FF_i \rangle_{ij} = \left\langle \left(\sqrt{\frac{N_i}{N_i - 1}} \frac{n_{ij} - \bar{n}_i}{\sqrt{\bar{n}_i}} \right)^2 \right\rangle_{ij}$$

where angular brackets $\langle\ \rangle_{ij}$ indicate average over all trials of all conditions (neuron and cue), N_i is the number of trials in condition i (corresponding to a specific neuron and cue), N is the total number of conditions, N_T is the total number of trials in all conditions ($N_T = \sum N_i$), $\bar{n}_i$ is the mean spike count in condition i and n_{ij} is the spike count in trial j of condition i. This calculation yields an average of the Fano factors of individual conditions FF_i in the database, weighted by the total number of trials in each condition N_i, and is therefore a more robust estimator of the population Fano factor FF than the unweighted average over conditions.

Spike count correlations were calculated as the Pearson correlation coefficient between the spike counts of pairs of neurons, and then averaged over neurons.

All analyses were carried out in Matlab, using the CircStat toolbox[55] to perform circular statistics.

Statistical methods. We applied parametric tests (t test, ANOVA or Harrison-Kanji test for circular data) to validate our hypotheses whenever our data satisfied the assumptions of normality and homoscedasticity (Lilliefors test of normality, $P > 0.05$, and Levene's test for equality of variances, $P > 0.05$, respectively). For two of the ANOVA analyses, we accepted mild deviations from the assumptions, as they were unlikely to affect the strong effect reported by the ANOVA ($P < 0.005$; **Supplementary Fig. 4**). When tests comparing one or two samples failed to meet the parametric test assumptions, we applied the non-parametric Wilcoxon test or a permutation test when normality was not met, and Welch's t test for heteroscedastic data. Fano factors and tuning strength T were Box-Cox transformed to correct skewness (exponent range, 0.22–0.28) before testing. Pearson correlations were Fisher-transformed before population tests. Pairwise comparisons critically predicted by the model were also re-tested with permutation tests to validate near-threshold t test hypothesis rejections (**Figs. 6** and **7**). When the model prediction identified the sign of the comparison we used one-sided tests, and this is explicitly indicated in the text. Paired tests are used to compare measurements within neurons; in ANOVAs this is accomplished by using a mixed-effects design with neuron as random factor, nested in the monkey factor. Bootstrap estimates of the standard error of the Fano factor are calculated as the s.d. of Fano factors evaluated in 1,000 bootstrap samples obtained by randomly resampling with replacement from the spike counts for all cues, independently for each neuron. In all analyses, outliers beyond 3 s.d. of the population mean were removed for population tests and descriptive statistics are indicated by mean ± s.e.m.

Computational models. We tested different network representations for memory maintenance in three computational network models, the bump attractor network, the discrete attractor network and the decaying bump network. We provide Matlab code for these models, including all relevant parameters, as **Supplementary Codes 1–3.** In brief, the models were firing-rate network models

doi:10.1038/nn.3645

with N = 512 excitatory neurons and 512 inhibitory neurons labeled by an angle θ_i used for decoding, characterized by an input-output function function $r = \phi(I)$, mutually coupled via all-to-all connectivity matrices W_{EE}, W_{EI}, W_{IE}, W_{II} and subject to a white noise Gaussian input $\xi(t)$ of s.d. σ:

$$\tau_E \frac{dr_i^E}{dt} = -r_i^E + \phi\left(\sum_j \left(W_{EE}^{ij} r_j^E - W_{EI}^{ij} r_j^I\right) + I_m + I_0^E\right) + \sigma_E \xi(t)$$

$$\tau_I \frac{dr_i^I}{dt} = -r_i^I + \phi\left(\sum_j \left(W_{IE}^{ij} r_j^E - W_{II}^{ij} r_j^I\right) + I_0^I\right) + \sigma_I \xi(t)$$

Connectivity matrices were all homogeneous ($W^{ij} = W_0$) except for connectivity among excitatory neurons, which had different patterns depending on the network model: for the bump attractor network W_{EE}^{ij} was a circular Gaussian function of $i - j$ (**Fig. 8a**), for the discrete attractor network W_{EE}^{ij} took one of five possible values depending on which two of eight populations neurons i and j belonged to (**Fig. 8a**), for the decaying bump network W_{EE}^{ij} was zero so no recurrent excitation was included. Instead, the decaying bump network included one intrinsic current in excitatory neuron that provided slowly decaying depolarization during the delay period

$$\tau_m \frac{dI_m}{dt} = -I_m + \alpha_m \frac{r^E}{1 + e^{-2\left(r^E - 2\right)}}$$

for the other two network models $I_m = 0$. We simulated a task mimicking the behavioral task in the data: 1-s pre-stimulus, 500-ms stimulus presentation (increased current input to subset of neurons θ_i near stimulus location θ_s) and 3-s delay period where models evolved autonomously based on their dynamics. At the end of the delay period, the behavioral response was decoded using a population vector decoder

$$\hat{\theta} = \arg\left(\sum_{j=1}^{N} r_j^E e^{i\theta_j}\right)$$

and a global hyperpolarizing injected current erased selective network activity. Sample trials for each network model are illustrated in **Supplementary Videos 1–3**.

For each model, we obtained a data set of neuron firing rates that mimicked our experimental data set: 200 neurons, with eight different cues (θ_s = 0°, 45°, 90°, 135°, 180°, 225°, 270° and 315°) and ten independent trials per cue were sampled from a total of 16,000 independent trial simulations, and the behavioral response decoded from the population activity at the end of the delay was recorded. We applied the analyses of **Figures 3** and **4** to these data sets in **Figure 8**.

Although these network models replicated the qualitative features of the experimental data set, specific firing rate values, heterogeneity of tuning and near-Poisson spiking statistics could not be matched quantitatively in our simple firing rate network models (**Fig. 8**). For this reason, we further tested our analyses on surrogate data from two computational coding models that could match quantitatively the experimental data of **Figure 1**, the bump attractor model and the decaying bump model (**Supplementary Figs. 5** and **6**). In both coding models, spike trains for individual trials were derived as inhomogeneous Poisson processes with time-varying firing rate $\lambda(t)$ described by an evolving bump of activity. In both cases, the bump shape was based on a von Mises distribution (a circular Gaussian) so that the firing rate of neuron i during one trial took the form

$$\lambda_i(t, \theta_i) = r_{\min} + \left(r_{\max} - r_{\min}\right) \frac{e^{\kappa(t)\cos\left(\theta_i - \theta(t)\right)} - e^{-\kappa_0}}{e^{\kappa_0} - e^{-\kappa_0}}$$

where θ_i is the neuron"s preferred location and $\theta(t)$ is the location of the bump center. The parameter $\kappa(t)$ determines the width of the bump. For large $\kappa(t)$, the s.d. of the von Mises distribution is approximately $w(t) = 180/\left(\pi\sqrt{\kappa(t)}\right)$, so we refer to $w(t)$ as the bump width. When $w(t) = w_0$, where $w_0 = 180/\left(\pi\sqrt{\kappa_0}\right)$, the firing rate equation is normalized so that the parameters $r_{\min}$ and $r_{\max}$ determine each neuron"s lowest and highest firing rates, respectively.

In the bump attractor model, the bump width was fixed at $w(t) = w_0 = 35°$ for all trials. The variation across trials was due to diffusion in the bump center $\theta(t)$. In each trial, the bump center was initialized at the location of the cue presentation θ_s at the beginning of the delay period. During the delay period, the bump center evolved according to

$$\frac{d\theta}{dt} = \sigma\eta(t)$$

where $\eta(t)$ is Gaussian white noise and the diffusion magnitude σ = 4.04 was chosen so that the bump center had a s.d. of 7° at the end of a 3-s delay period, similar to experimental data (**Fig. 1b**). For each neuron, the minimum and maximum firing rates were randomly drawn from Gaussian distributions so that $r_{\min} = 7 \pm 1$ Hz and $r_{\max} = 14 \pm 3.4$ Hz (mean ± s.d.), with the constraint that $r_{\min} < r_{\max}$.

In the decaying bump model, the bump center was fixed at the cue position $\theta(t) = \theta_s$ and its width was initially the same as in the bump attractor model $w(t) = w_0 = 35°$. However, in each trial the bump width increased linearly with time:

$$\frac{dw}{dt} = \alpha$$

where the speed α was chosen randomly for each trial from a gamma distribution with mean of 17.5 ° s^{-1} and an s.d. of 5.83 ° s^{-1}. The parameters $r_{\min}$ and $r_{\max}$ were randomly drawn from Gaussian distributions so that $r_{\min} = 7 \pm 1$ Hz and $r_{\max} = 14 \pm 3.4$ Hz (mean ± s.d.), with the constraint that $r_{\min} < r_{\max}$. The parameters $r_{\min}$ and $r_{\max}$ specify the maximum and minimum firing rates only for the initial bump width when $w(t) = w_0$; the widening of the bump decreases the range of firing rates. This choice of parameters mimicked the experimental neural data and behavioral reports of **Figure 1** quantitatively.

For each of the two models, we obtained a data set of neuron spike trains that mimicked our experimental data set: 200 neurons, with eight different cues (θ_s = 0°, 45°, 90°, 135°, 180°, 225°, 270° and 315°) and ten independent trials per cue were sampled from a total of 16,000 independent trial simulations. Trials consisted in a fixation period of 1 s (homogeneous Poisson at rate $r_{\min}$), a cue period of 0.5 s (formulas above with fixed $\theta(t) = \theta_s$ and $w(t) = w_0$) and a delay period of 3 s (time-varying formulas above).

For each individual trial that we simulated, we could also extract a behavioral response θ_{out} based on the firing rate at the end of the delay. To this end, we extracted Poisson spike counts for N = 4,000 neurons with evenly-spaced angles θ_i. Fixing the firing rates to those calculated at the end of the delay, we counted spikes for 0.5 s. From these spike counts $\{n_i, i = 1 \ldots N\}$ we computed the population vector $\mathbf{V} = \sum_{i=1}^{N} n_i e^{i\theta_i}$, from which we extracted the decoded behavioral response $\theta_{out} : \mathbf{V} = |V| e^{i\theta_{out}}$. We treated this response similarly to the behavioral response of the monkey in our experimental data set.

51. Constantinidis, C., Williams, G.V. & Goldman-Rakic, P.S. A role for inhibition in shaping the temporal flow of information in prefrontal cortex. *Nat. Neurosci.* **5**, 175–180 (2002).
52. Constantinidis, C. & Goldman-Rakic, P.S. Correlated discharges among putative pyramidal neurons and interneurons in the primate prefrontal cortex. *J. Neurophysiol.* **88**, 3487–3497 (2002).
53. Jin, D.Z., Dragoi, V., Sur, M. & Seung, H.S. Tilt aftereffect and adaptation-induced changes in orientation tuning in visual cortex. *J. Neurophysiol.* **94**, 4038–4050 (2005).
54. Compte, A. & Wang, X.-J. Tuning curve shift by attention modulation in cortical neurons: a computational study of its mechanisms. *Cereb. Cortex* **16**, 761–778 (2006).
55. Berens, P. CircStat: a MATLAB toolbox for circular statistics. *J. Stat. Softw.* **31**, 1–21 (2009).